THE TONUS CFD CODE FOR HYDROGEN RISK ANALYSIS: PHYSICAL MODELS, NUMERICAL SCHEMES AND VALIDATION MATRIX

S. Kudriakov[1], F. Dabbene[1], E. Studer[1], A. Beccantini[1], J.P. Magnaud[1], H. Paillère[1]
A. Bentaib[2], A. Bleyer[2], J. Malet[3] and C. Caroli[2]
[1] CEA Saclay, Nuclear Energy Division, 91191 Gif-sur-Yvette Cedex, France
[2] Institut de Radioprotection et de Sureté Nucléaire, Reactor Safety Division, BP 17, 92262 Fontenay-aux-Roses Cedex, France
[3] Institut de Radioprotection et de Sureté Nucléaire, Plant, Laboratories, Transport and Waste Safety Division, 91192 Gif-sur-Yvette, France

Abstract

The French Atomic Energy Commission (CEA) and the Radiation protection and Nuclear Safety Institute (IRSN) are developing a hydrogen risk analysis code (safety code) which incorporates both lumped parameter (LP) and computational fluid dynamics (CFD) formulations. In this paper we present the governing equations, numerical strategy and schemes used for the CFD approach. Typical numerical studies will be presented for hydrogen distribution and combustion applications in realistic large geometries.

1. Introduction

The TONUS code is the French hydrogen risk analysis code developed by CEA and IRSN over the last decade, to model hydrogen release, distribution and combustion in a PWR reactor containment. The code has both multi-compartment lumped-parameter and CFD formulations, but the present paper will only focus on the CFD part of the code, describing the physical models that have been implemented, the numerical algorithms that have been developed, and the extensive matrix of experiments used for validation purposes. Since the objective of the code is to be applied to real plant applications such as EPR studies, numerical considerations such as mesh size and CPU run-time constrained the choice of physical models and numerical algorithms. On the other hand accuracy requirements and the need to apply to the greatest extent possible ”best practice guidelines” when performing calculations were also taken into account when developing and validating the code.

The first part of the paper will briefly describe the physical models and numerical schemes implemented in the version v2006.1 of the TONUS CFD code. For the distribution part, a low Mach number multi-component Navier-Stokes solver was developed, incorporating two types of turbulence models - mixing length and standard k-e models, and wall condensation models based on the heat and mass transfer analogy - Chilton-Colburn correlations. Heat transfer to the structures is modeled by coupling the CFD equations to 3D heat conduction equations. Mitigation systems such as passive autocatalytic recombiner systems are also modeled and coupled to the CFD solver. As far as combustion is concerned, different types of models have been developed to cover slow deflagration regimes, accelerated flames and detonation and implemented in a fully compressible flow solver able to simulate shock wave propagation. Numerical algorithms suited to the various flow regimes - low Mach number flows characteristic of the hydrogen distribution phase up to high speed flows associated with hydrogen combustion - have been developed and optimized to perform efficiently on the single processor platforms (Linux or Windows PC) on which the TONUS code was developed.

In the second part of the paper, we will review in detail the test cases which form the basis of the validation of the TONUS CFD code and identify the advantages and deficiencies of the models. The strategy for the validation of the code followed a progressive approach in terms of physical phenomena, from

Separate Effect Tests (SET) to Coupled Effect Tests (CET). Much of the data used for the validation of the distribution models was produced in the 7 m^3 TOSQAN and 100 m^3 MISTRA containment facilities operated by IRSN and CEA respectively and which were specially developed to produce high quality detailed data suitable for CFD code validation with well-controlled boundary conditions and a dense mapping of sensors in the volumes. Test data from the ISP-47 exercise is an example of such data. Besides TOSQAN and MISTRA data, tests from AECL's Large Scale Gas Mixing Facility (LSGMF), PHEBUS, ThAI and PANDA facilities were used for validation purposes. Validation of mitigation models (spray, recombiners) will also be described in the paper. For the combustion part of the code, use was made of large scale hydrogen combustion tests which are representative of containment geometries such as Battelle, HDR and RUT tests which cover all the combustion regimes from slow deflagrations to detonations. More detailed data produced in the IRSN-sponsored ENACCEF facility is also being used to investigate accelerated flame regimes. It is also to be noted that many of the TONUS validation cases have been selected in the OECD Containment Code Validation Matrix (CCVM) and are therefore considered as "mandatory" validation cases for containment codes.

The paper will conclude with a description of on-going work including further code development and validation cases, interpretation of new MISTRA and TOSQAN tests and plant applications including EPR calculations.

2. Physical Modelling

The general equations for modelling containment flows, from H_2 distribution to combustion, are the multicomponent (N species) compressible Navier-Stokes equations which express the conservation of mass, the mass conservation for species l ($l = 1, ..., N-1$), conservation of momentum and energy. In divergence form they read:

$$\frac{\partial \rho}{\partial t} + \nabla \cdot (\rho \mathbf{u}) = 0 \tag{1}$$

$$\frac{\partial \rho_l}{\partial t} + \nabla \cdot (\rho_l(\mathbf{u} + \mathbf{u_{dl}})) = \dot{\omega}_l \tag{2}$$

$$\frac{\partial \rho \mathbf{u}}{\partial t} + \nabla \cdot (\rho \mathbf{u} \otimes \mathbf{u} + p\mathbf{I}) = \nabla \cdot \tau + \rho \mathbf{g} \tag{3}$$

$$\frac{\partial \rho E}{\partial t} + \nabla \cdot (\rho \mathbf{u}(E + \frac{p}{\rho})) = \nabla \cdot (\tau \cdot \mathbf{u} - \mathbf{q}) + \rho \mathbf{g} \cdot \mathbf{u} \tag{4}$$

where ρ is the mixture density, ρ_l is the density of species l ($l = 1, ..., N-1$), p is the pressure, $\mathbf{u}$ is the velocity vector, $\mathbf{I}$ is the identity tensor, $\mathbf{g}$ is the acceleration due to gravity, τ is the viscous tensor, E is the specific total energy, $\mathbf{u_{dl}}$ is the diffusion velocity, $\dot{\omega}_l$ is the reaction rate of species l and $\mathbf{q}$ is the heat flux vector.
The system is closed by the thermal equation of state

$$p = \rho R T \tag{5}$$

where R is the gas mixture constant and T is the temperature, Fick's law for the species diffusion

$$\mathbf{u_{dl}} \rho_l = -\rho D_l \nabla Y_l \tag{6}$$

where $Y_l = \frac{\rho_l}{\rho}$ is the species l mass fraction and D_l is the diffusion coefficient of species l into the gas mixture, and caloric equation of state which relates the specific internal energy e to the temperature T, i.e.

$$e(T) = \sum_{l=1}^{N} Y_l e_{0l} + \int_{T_0}^{T} C_v(T')dT' \tag{7}$$

where C_v is the mixture specific heat capacity at constant volume,

$$C_v(T) = \sum_{l=1}^{N} Y_l C_{vl}, \tag{8}$$

and e_{0l} the internal energy of species l at temperature T_0. Similar expressions relate the specific enthalpy h of the mixture to the heat capacities at constant pressure C_{pl} of the species and to the temperature. A standard expression for the heat flux is assumed and is given by

$$\mathbf{q} = -\lambda \nabla T - \sum_{l=1}^{N} \rho D_l h_l \nabla Y_l \tag{9}$$

where λ is the thermal conductivity, and

$$h_l = \triangle h_{f,l} + \int_{T_0}^{T} C_{pl}(T')dT' \tag{10}$$

where $\triangle h_{f,l}$ is the specific enthalpy of formation for the component l at the temperature T_0.

These equations are further simplified for the various flow regimes that characterise containment flows in the event of a severe accident. In detonation regimes for example, when the flow propagation is governed by the motion of reactive shock waves, it is a valid assumption to neglect viscous and heat conduction effects. This leads to an approximation of the Navier-Stokes equations known as the Euler equations. For low speed flows, on the other hand, another approximation of the Navier-Stokes equations valid for low Mach number flows is used, for accuracy and efficiency reasons. This is discussed in the following paragraph.

2.1. Low Mach number model

The thermal-hydraulic flows associated with steam and hydrogen release and mixing are mainly low Mach number flows. A low Mach number compressible solver can be constructed on the basis of an asymptotic analysis of the compressible Navier-Stokes equations in the small Mach number limit. The acoustic waves are filtered, thus avoiding the stiffness problem completely [12]. As a result, the pressure can be split into a uniform time-dependent thermodynamic pressure $P(t)$ and a dynamic pressure $p'(\mathbf{r}, t)$ which is $O(M^2)$, where M is the Mach number,

$$p(\mathbf{r}, t) = P(t) + p'(\mathbf{r}, t) \tag{11}$$

The resulting equations are written in non-conservative, Favre-averaged form (without chemical reactions) as

$$\overline{\rho} = \frac{1}{\Omega}\int_{\Omega} \rho d\Omega \tag{12}$$

$$P = \frac{\overline{\rho}\Omega}{\int_{\Omega} \frac{1}{RT} d\Omega} \tag{13}$$

$$\rho\left[\frac{\partial \mathbf{u}}{\partial t} + \mathbf{u}\cdot\nabla\mathbf{u}\right] = -\nabla p' + \nabla\cdot(\tau + \tau_t) + \mathbf{g}(\rho - \overline{\rho}) \tag{14}$$

$$\frac{1}{\gamma - 1}\Omega\frac{dP}{dt} = Q_j H_j - \int_{\partial\Omega}(\mathbf{q}\cdot\mathbf{n})dA \tag{15}$$

$$\rho C_p\left[\frac{\partial T}{\partial t} + \mathbf{u}\cdot\nabla T\right] = \frac{dP}{dt} + \nabla\cdot[(\lambda + \lambda_t)\nabla T] \tag{16}$$

$$\frac{\partial \rho_l}{\partial t} + \nabla\cdot(\rho_l \mathbf{u}) = \nabla\cdot\left[(\rho D_l + \frac{\mu_t}{Sc_t})\nabla Y_l\right] \tag{17}$$

where $\overline{\rho}$ is the mean density, τ_t the turbulent stress tensor, γ the isentropic coefficient of the mixture, Ω the volume, Q_j the injected mass flow rate, H_j the injected enthalpy, μ_t the turbulent dynamic viscosity, Sc_t the turbulent Schmidt number, and λ_t the turbulent thermal conductivity.

We discretise the above set of equations using the finite element method. The time discretisation is obtained by a semi-implicit second order (BDF2) incremental projection method [10]. In a first step, the momentum and energy equations are solved using the pressure variable from the previous time step. As a second step, the pressure equation is solved using the incremental algorithm.

2.2 High speed flow model

In a detonation regime the reactive mixture is heated by compression across a strong shock. Since in a such type of flow the Reynolds number is very high and the duration of the flow is very short, viscous and heat conduction effects as well as buoyancy forces can be neglected in (1)-(4), and the phenomenon is simulated by solving the reactive Euler equations.

The Finite Volume method is used in which the Euler equations are first expressed in integral form as

$$\frac{d}{dt}\int_{\Omega}\mathbf{U}d\Omega+\int_{\partial\Omega}(\mathbf{J}\cdot\mathbf{n})dA=\mathbf{S} \tag{18}$$

where Ω is a control volume, $\partial\Omega$ is the boundary of Ω, $\mathbf{U}$ is the vector of conserved variables, $\mathbf{J}$ is the matrix of convective fluxes, $\mathbf{n}$ is the outward unit vector normal to the surface $\partial\Omega$, dA is an area element and $(\mathbf{J}\cdot\mathbf{n})dA$ is the flux component normal to the boundary $\partial\Omega$ discretised using Riemann-type solvers (Van Leer-Hanel, Shock-Shock, AUSM+). Second-order space and time approximations are obtained by the predictor-corrector method of Van Leer-Hancock and the MUSCL approach [3].

2.3. Turbulence modeling

In the TONUS code there are two turbulence models available: a mixing length model and a $k-\epsilon$ model.
Mixing length model
For wall-bounded turbulent flows, the eddy viscosity must vary with distance from the wall, hence the addition of the concept of a 'mixing length'. In this model we assume that the eddy viscosity μ_t is linked to turbulence scales.
A turbulent viscosity μ_t is obtained from a turbulent length scale l_m using the expression

$$\mu_t=\rho l_m^2\cdot||\frac{1}{2}(\nabla\mathbf{u}+\nabla^T\mathbf{u})||. \tag{19}$$

$k-\epsilon$ model
The model consists of two equations, one for the turbulent kinetic energy k and one for the rate of dissipation of the turbulent energy, ϵ. These equations are:

$$\rho\left[\frac{\partial k}{\partial t}+\mathbf{u}\cdot\nabla k\right] = \nabla\cdot\left\{(\mu+\frac{\mu_t}{\sigma_k})\nabla k\right\}+P_k+G-\rho\epsilon \tag{20}$$

$$\rho\left[\frac{\partial \epsilon}{\partial t}+\mathbf{u}\cdot\nabla \epsilon\right] = \nabla\cdot\left\{(\mu+\frac{\mu_t}{\sigma_\epsilon})\nabla \epsilon\right\}+C_{\epsilon1}(1+C_{\epsilon3}S)(P_k+G)\frac{\epsilon}{k}-C_{\epsilon2}\rho\frac{\epsilon^2}{k} \tag{21}$$

where $S=0$ if the thermal stratification is instable ($\frac{\partial T}{\partial z}<0$), $S=-\frac{G}{P_k+G}$ otherwise, and

$$P_k = \mu_t\left[(\nabla\mathbf{u}+\nabla^T\mathbf{u}):\nabla\mathbf{u}-\frac{2}{3}(\nabla\cdot u)^2\right]-\frac{2}{3}\rho k(\nabla\cdot\mathbf{u}) \tag{22}$$

$$G = \frac{\mu_t}{\sigma_t}\mathbf{g}\cdot\nabla T \tag{23}$$

and

$$\mu_t = \rho C_\mu \frac{k^2}{\epsilon} \tag{24}$$

The coefficients used in the TONUS code are

C_μ	$C_{\epsilon 1}$	$C_{\epsilon 2}$	$C_{\epsilon 3}$	σ_k	σ_ϵ	σ_t
0.09	1.41	1.92	0.8	1.0	1.3	0.7

2.4. Condensation modelling

In containment thermal-hydraulics, steam condensation on the walls of the containment vessel is an important mass and energy sink. The model implemented in the TONUS code is a model of steam diffusion through a mass boundary layer based on heat and mass transfer analogy (Chilton-Colburn type) [5].

We do not explicitly model a liquid film at a wall. Instead, we assume that the vapour is in direct contact with the wall. We define the heat flux ϕ between the gas (first cell next to the wall with the gas temperature and pressure T_g and P respectively) and the associated condensing wall (under the temperature T_w):

$$\phi = h_{tot}(T_g - T_w) \tag{25}$$

where h_{tot} $(W/m^2/K)$ is the sum of the convective and the condensation heat transfer.

In the Chilton-Colburn correlation the convective part is modeled by a classical correlation valid for turbulent free convection along a vertical plate:

$$h_{conv} = 0.13\lambda \left[\frac{g}{\nu^2} \frac{(\rho_w - \rho_g)}{\rho_g} \right]^{\frac{1}{3}}, \qquad \nu = \frac{\mu}{\rho} \tag{26}$$

where $\rho_w = \rho_{steam} + \rho_{n.c.gases}$ (n.c. = non-condensable gases), ρ_{steam} is taken at T_w and $P_{sat}(T_w)$ while $\rho_{n.c.gases}$ taken at T_w and $(P - P_{sat}(T_w))$.

The condensation part is constructed with a mass transfer coefficient k_c (m/s) based on a heat and mass transfer analogy:

$$h_{cond} = \alpha k_c \left(\frac{h^{steam} - h^{liq}}{T_g - T_w} \right) (\rho_g^{steam} - \rho_w^{steam}) \tag{27}$$

$$k_c = h_{conv} \frac{D_{steam}^{2/3} \nu^{1/3}}{\lambda} \tag{28}$$

where α is a user-defined parameter, taken to be 1.0 in the TONUS code, h is the enthalpy, D_{steam} is the diffusion coefficient of steam in the gas mixture (m^2/s) and $(h^{steam} - h^{liq})$ is the phase transition latent heat.

Based on the theory of the condensation on the liquid film in the presence of noncondensable gases, one can obtain the following form of the mass transfer coefficient k_c:

$$k_c = h_{conv} \frac{D_{steam}^{2/3} \nu^{1/3}}{\lambda} \left(\frac{1}{1 - Y_w^{steam}} \right) \tag{29}$$

2.5. Passive autocatalytic hydrogen recombiner

In the event of a severe nuclear accident, a hydrogen recombiner decreases the hydrogen density in the containment by way of a catalytic reaction with oxygen. The oxydation occurs on the recombiner plates which are heated by the chemical reaction. This creates a vertical natural convection flow inside the recombiner vessel which supplies the recombiner with hydrogen and oxygen.

For the recombiner we use a lumped parameter approach, while the containment fluid volume as well as the inlet and the outlet of the recombiner are meshed (see figure 1). As a consequence, the recombiner model has to be supplied with space-averaged boundary conditions.

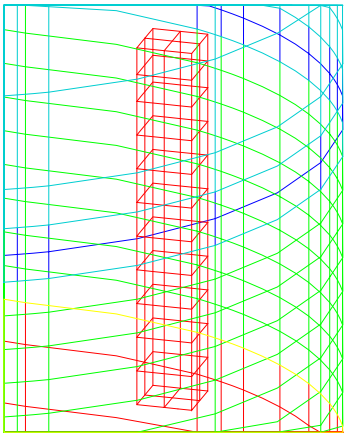

Figure 1: Example of exterior of a recombiner meshing.

It is assumed that the recombiner vessel does not exchange heat with the ouside gas mixture and the flow inside the recombiner is steady. To calculate the hydrogen mass flow rate of the catalytic reaction $\dot{m}_{H_2}$, we use the manufacturer (Siemens) correlation.

$$\dot{m}_{H_2} = \min\left(X^i_{H_2}, 2X^i_{O_2}, 0.08\right)(A\,P + B)\tanh(X_{H_2} - X^{ref}_{H_2}) \tag{30}$$

where $X^{ref}_{H_2} = 0.005$, A and B are coefficients that depend on the recombiner type; P is the total pressure; $X^i_{H_2}$ and $X^i_{O_2}$ are the inlet hydrogen and oxygen molar fractions. The system describing the gas flow inside the recombiner includes the mass balances for each gas component, the mixture momentum

equation and the energy balances for the recombiner plates and the gas mixture. These equations are given by

$$Y^o_{N_2} = Y^i_{N_2} \quad (31)$$

$$Y^o_{H_2} = Y^i_{H_2} - \frac{\dot{m}_{H_2}}{\dot{m}} \quad (32)$$

$$Y^o_{O_2} = Y^i_{O_2} - \frac{W_{O_2}}{2W_{H_2}}\frac{\dot{m}_{H_2}}{\dot{m}} \quad (33)$$

$$Y^o_{H_2O} = Y^i_{H_2O} + \frac{W_{H_2O}}{W_{H_2}}\frac{\dot{m}_{H_2}}{\dot{m}} \quad (34)$$

$$\left(K^i + k_{loss}\frac{L}{D_h} + K^o\right)\frac{1}{2}\frac{\dot{m}^2}{\overline{\rho}s^2} = g\left((\rho_{ext} - \overline{\rho})L + (\rho_{ext} - \rho^o)L_{ch}\right) \quad (35)$$

$$\dot{m}_{H_2}\Delta H = m_s C_{p_s}\frac{dT_s}{dt} + S_s h\left(T_s - T^i\right) \quad (36)$$

$$\dot{m}\overline{C}_p\left(T^o - T^i\right) = S_s h\left(T_s - T^i\right) \quad (37)$$

where W_j is the component j molar mass, Y^i_j (resp. Y^o_j) is the inlet (resp. outlet) mass fraction of component j, $\dot{m}$ is the recombiner mass flow rate, K^i is the inlet singular pressure loss coefficient, k_{loss} is the regular pressure loss coefficient, K^o is the outlet singular pressure loss coefficient, s is the free cross section in the recombiner sections, D_h is the flow path diameter in the recombiner sections, ΔH is the specific enthalpy of the hydrogen combustion reaction, m_s, C_{p_s}, T_s and S_s are respectively the mass, the heat capacity, the temperature and the surface of the recombiner sections, h is the heat exchange coefficient between the sections and the gas; T^i is the inlet gas temperature, $\overline{C}_p = \frac{1}{2}(C^i_p + C^o_p)$ is the "average" gas heat capacity and T^o is the outlet gas temperature. It is assumed that density outside the recombiner is equal to density at the recombiner inlet ($\rho_{ext} = \rho^i$).

2.6. Combustion modelling

The combustion model provides the reaction rates $\dot{\omega}_l$ for the premixed gas chemical reaction. The rates appear in the source terms of the species transport equations (2). The reaction of hydrogen oxidation can be written in a global form as:

$$2H_2 + O_2 \xrightarrow{\dot{\omega}} 2H_2O \quad (38)$$

where $\dot{\omega}$ is the global reaction rate which, although not representative of the kinetic mechanism of the reaction and thus not theoretically defined, can be 'modelled' and used to simulate combustion in engineering applications. It is unfortunately not possible to use a single expression for $\dot{\omega}$ to model the hydrogen-oxygen reaction in all conditions (laminar or turbulent deflagrations, detonations) and in this section we shall describe different choices that have been made for the TONUS code.
Different combustion regimes are experienced as different flame characteristics observed during the deflagration. Shortly after ignition, the combustion is partly laminar. The reaction rate used in this case is the laminar 'Arrhenius' rate [17]:

$$\dot{\omega}_1 = C_f\left(\frac{\rho_{H_2}}{W_{H_2}}\right)\left(\frac{\rho_{O_2}}{W_{O_2}}\right)exp(-T_a/T) \quad (39)$$

where $C_f = 3.3 \times 10^5$ m^3/mol/s and T_a is the activation temperature, $T_a = 10^4$ K. In the fully turbulent regime the 'Eddy Break-Up' rate by [14] is utilized:

$$\dot{\omega}_2 = C_{EBU}\frac{\rho_{H_2}}{2W_{H_2}}\frac{\epsilon}{k}\left(1 - \frac{Y_{H_2}}{Y_{H_2,u}}\right) \quad (40)$$

where $Y_{H_2,u}$ is the mass fraction of hydrogen in the unburned region of the flow and C_{EBU} is the so-called 'Eddy Break-Up' constant. In the code we take $\dot{\omega} = max(\dot{\omega_1}, \dot{\omega_2})$

To model detonation, the Arrhenius global reaction rate ([9], [2]) is used in the TONUS code. It has the following form:

$$\dot{\omega} = A \cdot H(T - T_{th}) \cdot \rho_{H_2}^c \cdot \rho_{O_2} \cdot T^{-b} \cdot exp(-T_a/T) \tag{41}$$

where, for the test cases integrated in the validation matrix we use $A = 1.1725 \times 10^{14}$, $c = 2.0$, $b = 0.91$ and $T_a = 8310$ K. Here $H(T-T_{th})$ is the Heaviside's function with T_{th} being the threshold temperature. Another approach, the CREBCOM (CRiteria and Experimentally Based COmbustion Model) model [8], developed at the Kurchatov Institute, is specifically devoted to the study of combustion in geometries which are much larger than the characteristic dimensions of the physical phenomena involved. Thermal conduction and species diffusion, which are responsible for the propagation of deflagrations, are not modelled; their action is taken into account by introducing an experimentally derived correlation source term into the Euler equations [8].

The reaction rate is written for the progress variable ξ

$$\xi(\vec{r}, t) = \frac{Y_{H_2}(\mathbf{r}, t) - Y_{H_2,u}(\mathbf{r}, t)}{Y_{H_2,b}(\mathbf{r}, t) - Y_{H_2,u}(\mathbf{r}, t)} \tag{42}$$

where the indices u and b refer to the 'unburned' and 'burned' mixture (i.e. the mixture before and after combustion) respectively. It has the following form:

$$\dot{\omega}_\xi = \rho \frac{K_0}{\triangle x} \cdot f_{criter} \tag{43}$$

where K_0 is a parameter, $\triangle x$ the mesh dimension and f_{criter} is the criterion function which serves to track the flame front. The reaction rate (43) can be applied for laminar and turbulent deflagrations and for detonations.

3. TONUS Validation Matrix

3.1. A comprehensive matrix

The TONUS code has been validated on a number of test cases covering such physical phenomena as gas distribution in closed volumes, combustion of gaseous mixtures, sprays and distribution with passive autocatalytic recombiner present. The test cases are summarised in Table 1.

3.2. Selected example: ISP47 MISTRA Phase 1 [16]

The MISTRA program [15] is conducted in the framework of studies of severe accidents occuring in Pressurized Water Reactors (PWR), and is focussed on the hydrogen risk. The main objective is to support modeling and validation of multi-dimensional thermal-hydraulic codes devoted to containment analysis, by providing detailed experimental data. The scale of the facility is suitable for turbulent and convective flows with steam condensation and the instrumentation has been designed to characterize 3D multi-component flows.

The MISTRA facility is a stainless steel containment of 99.5 m^3. The internal diameter (4.25 m) and the height (7.3 m) have been chosen to correspond to a linear length scale ratio of 0.1 with a typical French

Distribution	**AECL LSGMF**	3D air/He
	Phebus FPT0	3D air/steam/H2
	Phebus FPT1	3D air/steam/H2
	MISTRA Helium tests	2Daxi air/He
	MISTRA ISP47 Phase 1	2Daxi air/steam
	MISTRA ISP47 Phase 2	2Daxi air/steam/He
	MISTRA ISP47 Phase 1	3D air/steam
	MISTRA M1	2Daxi air/steam
	MISTRA M2	2Daxi air/steam
	MISTRA M3	3D air/steam
	MISTRA MICOCO	2Daxi air/steam
	TOSQAN 1,2,3,6,7,8,9b	2Daxi air/steam
	ISP47 TOSQAN Phase 1	3D air/steam
	MAEVA mock-up	3D air/steam
	ThAI preliminary calc.	3D air/steam
	PANDA SETH Test 17	3D air/steam
Distribution / Spray model	**TOSQAN 101**	2Daxi air/steam + spray
Distribution / Recombiners	**KALI 8 test**	3D + recombiner
Combustion	**Driver MC012**	2D fast flame
	HYCOM HYC01	3D fast flame
	RUT STM4	2D detonation
	HDR E12.3.2	3D slow flame
	BMC Ex29	3D slow flame

Table 1: TONUS validation matrix

PWR containment. The vessel itself is not temperature regulated but preheated by steam condensation and thermally insulated with 20 cm of rock wool.

Three condensers are inserted inside the containment, close to the vessel walls. A so-called “dead volume” behind the condensers exists, and during long term experiments spurious condensation can occur. The condensers consist of vertical pipes fitted together into 24 elementary cells. Each condenser has its own regulation circuit: internal and external collectors are specially designed to provide the cooling water with a most stable and uniform temperature (wall temperature difference less than 1^oC is achieved). Gutters are installed to collect and quantify the condensate. The external part of condensers is insulated with synthetic foam and viewing windows are installed for laser measurements. Spurious condensation is also quantified by condensate collecting at different locations: along the side walls of the containment, along the external part of the condensers and at the bottom. It should be noted that the collected water at the bottom of the containment is continuously measured and evacuated, though a sump can be created, if necessary.

A diffusion cone including a porous media and fitted with a removable cap is designed for gas injection and steam/gas mixing. Different injection diameters are allowed to cover a large range of Richardson numbers (covering jet and plume regimes). It also ensures a flat velocity profile and is set up in the central position (though non-centered position is possible). Injection gas flow rates are controlled and measured with sonic nozzles that ensure a contant value independent of the downward operating conditions. The different gases can be heated up to 200^oC which is the design temperature of the facility.

The test proposed for the **International Standard Problem 47** (ISP 47) is a coupled effect test that aims to reproduce the main phenomena occuring during an accidental situation relevant for hydrogen risk. The test is decomposed into four successive steps:

- (i) **Preheating step** due to steam injection into the containment initially full of air at 20^oC and 1 bar in order to heat-up the steel structures.
- (ii) **Air/steam steady state (Phase 1)** defined from the equilibrium between the injected (0.13 kg/s at 200^oC) and the condensed steam mass flow rate on temperature controlled walls (at 115^oC).
- (iii) **Air/steam/helium transient** due to steam and helium injection.
- (iv) **Air/steam/helium steady state (Phase 2)** defined from the equilibrium between the injected and the condensed steam mass flow rate on temperature controlled walls.

During the preheating step steam is injected with a 0.15 kg/s mass flow rate and the condensers are heated up from 20^oC to 134^oC with 0.4^oC/min heating rate. Initially at 20^oC, the injected steam reaches its nominal temperature - about 233^oC - after 30 minutes. This step stops when the pressure reaches 4.5 bar, the minimal containment internal wall temperature is higher than 130^oC and the containment internal wall temperature gradient is less than 5^oC.

After the preheating, the condensers are cooled from 134^oC to their nominal temperature, 115^oC, with a 3^oC/min cooling rate. The steam injection is stopped during this phase. When the condensers reach their nominal temperature, steam is injected centrally at the bottom at 200^oC and a mass flow rate of 0.13 kg/s. The steady state (Phase 1) is defined by the equilibrium between the injected steam mass flow rate and the condensed steam mass flow rate on the structures.

For the third step, steam is always injected at the same mass flow rate as in the previous phase and the helium injection starts. Helium injection is caracterised by a mass flow rate of 10.6 g/s for about 30 minutes. During the fourth step (Phase 2) the steady state is achieved with the same conditions as for the Phase 1.

Hereafter, we focus on the air/steam steady state (first and second steps of the sequence). In order to limit CPU time we directly set the air/steam steady state thermodynamic conditions without transfer studying. The condensers are at their nominal temperature 115^oC, the steam is injected on the central axis at the containment bottom at 200^oC and a mass flow rate of of 0.13kg/s. The steady state is defined by the equilibrium between the injected steam mass flow rate and the condensed steam mass flow rate on the structures, as well as the stability of all parameters - temperature, pressure and air/steam concentration.

The objective of the numerical experiment is twofold: **(1)** to study the grid sensitivity of the numerical solution by using meshes of 2D-axisimmetric geometry and full 3D geometry (see figure 2), and **(2)** to study the effect of the user parameters and the experimental uncertainties on the numerical solution.

The values of the global variables (pressure, mean temperature, rate of condensation on each condenser) as well as local values (temperature and velocity profiles along the predefined lines) computed on two grids are compared. From the results for the global variables (as well as for the local variables, not shown here) presented on the Table 2 we can conclude that 3D effects are not important, and for this test case one can use the 2D-axisimmetric geometry for validation purposes or sensitivity studies which are described in the following paragraphs.

The effect of the user parameters and the experimental uncertainty on the boundary conditions have to be quantified to provide a complete numerical study of this ISP exercise. The first step is to select the parameters and the variation ranges of each one. The second step is to define the variables to study. In the following paragraphs, these variables are called responses. Then, a methodology to perform the sensitivity study must be chosen. In our case, the Design-Of-Experiments technique [4] has been applied in order to optimise the number of calculations. Finally, the results have to be analysed.

The so-called parameters may have different origins. Five code-user parameters have been identified in the present TONUS modelling. One is related to the turbulence modelling: the mixing length (l_m), two

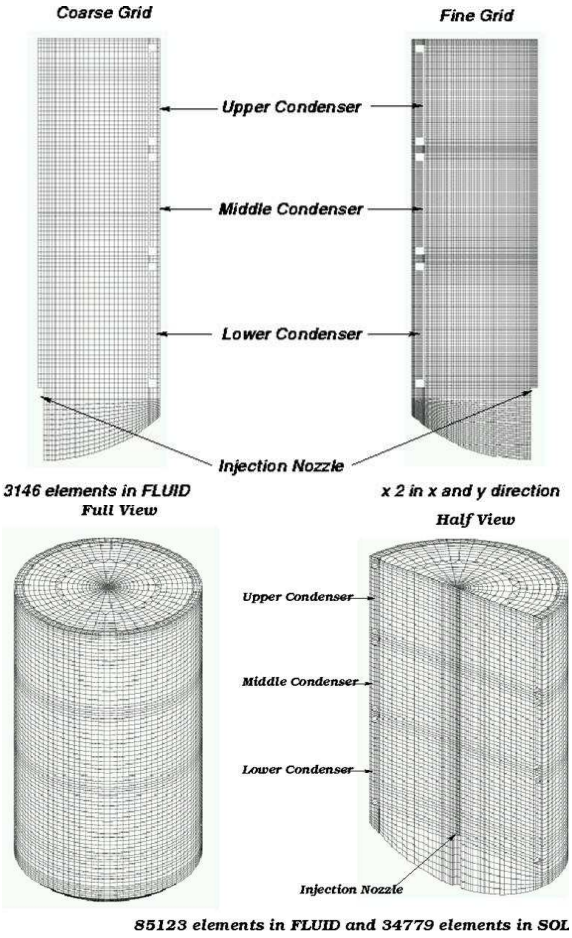

Figure 2: Grids used for the computation: 2D axisymmetric (coarse with $\triangle h = 7$ cm, top left; fine with $\triangle h = 3.5$ cm, top right) and full 3D ($\triangle h = 10$ cm, bottom).

Variables	**Experiment**	**2D** coarse	**2D** Err	**3D**
Total pressure (bar)	**3.342** $\pm$ **0.011**	3.303	0.34 %	3.29
Mean gas temperature (^{o}C)	**124.6** $\pm$ **0.5**	124.1	0.16 %	125.1
Q_{cond} (g/s) Lower	**37.5** $\pm$ **0.9**	32.66	1.75 %	32.2
Q_{cond} (g/s) Middle	**31.6** $\pm$ **0.8**	33.70	0.1 %	33.86
Q_{cond} (g/s) Upper	**40.8** $\pm$ **0.8**	41.99	1.6 %	42.63
Q_{cond} (g/s) Spurious	**17.4** $\pm$ **0.3**	21.66	0.31 %	21.37

Table 2: Comparison of the global variables computed on 3 meshes with experimental data. Err is the relative difference between the values obtained on the coarse and the fine grids, $Err = 100\% \cdot |()_{coarse} - ()_{fine}|/()_{fine}$.

Parameter	**Name**	**Variation (+/-)**
Initial Mass of Air	M_{air}	1.6%
Injection Steam Mass Flow Rate	Q_{st}	3 g/s
Injection Temperature	T_{inj}	4^{o}C
Upper Condenser Temperature	$T_{c,up}$	1^{o}C
Middle Condenser Temperature	$T_{c,m}$	1^{o}C
Lower Condenser Temperature	$T_{c,l}$	1^{o}C
Mixing Length	l_m	50%
External Heat Exchange Coefficient	h_{ext}	2 W/m^2/K
Convective Heat Transfer Coefficient along the Condensers	h_{conv}	40%
Steam Heat Capacity	$C_{p,s}$	6%
Latent Heat	h_l	6%

Table 3: Parameters selected for the sensitivity study.

are related to the heat transfer coefficient: convective heat transfer along the condensers h_{conv} and the external heat transfer coefficient h_{ext} (used to simulate the heat losses), and the last two are related to the perfect gas hypothesis used to model the steam: the steam heat capacity $C_{p,s}$ and the latent heat h_l. The second set of parameters is related to the uncertainties in the experimental boundary conditions. The selected parameters are related to the initial conditions in the MISTRA facility (initial mass of air M_{air}), the injection steam mass flow rate(Q_{st}), injection temperature (T_{inj}) and the surface temperature of the three condensers ($T_{c,up}$, $T_{c,m}$, $T_{c,l}$). The variations chosen for all these parameters are summarasied in Table 3 and they correspond to the estimated experimental uncertainty or engineering judgement of reasonable variations.

Eleven parameters have been selected for this sensitivity study. A screening approach has been adopted because at present time, only the first order is of interest, thus a linear response model (LRM) without interactions has been selected. For each response variable Y_i and the parameters X_i ($i = 1...11$), 12 coefficients called a_i, $i = 0...11$, of the linear response models have to be determined. This needs 12 calculations using the calculation matrix A (see eq. 44). The values of the parameters have been normalised in order to allow direct comparison of their weight.

$$\mathbf{A} = \begin{pmatrix} -1 & -1 & -1 & -1 & -1 & -1 & -1 & -1 & -1 & -1 & -1 \\ -1 & -1 & -1 & -1 & -1 & 1 & 1 & 1 & 1 & 1 & 1 \\ -1 & -1 & 1 & 1 & 1 & -1 & -1 & -1 & 1 & 1 & 1 \\ -1 & 1 & -1 & 1 & 1 & -1 & 1 & 1 & -1 & -1 & 1 \\ -1 & 1 & 1 & -1 & 1 & 1 & -1 & 1 & -1 & 1 & -1 \\ -1 & 1 & 1 & 1 & -1 & 1 & 1 & -1 & 1 & -1 & -1 \\ 1 & -1 & 1 & 1 & -1 & -1 & 1 & 1 & -1 & 1 & -1 \\ 1 & -1 & 1 & -1 & 1 & 1 & 1 & -1 & -1 & -1 & 1 \\ 1 & -1 & -1 & 1 & 1 & 1 & -1 & 1 & 1 & -1 & -1 \\ 1 & 1 & 1 & -1 & -1 & -1 & -1 & 1 & 1 & -1 & 1 \\ 1 & 1 & -1 & 1 & -1 & 1 & -1 & -1 & -1 & 1 & 1 \\ 1 & 1 & -1 & -1 & 1 & -1 & 1 & -1 & 1 & 1 & -1 \end{pmatrix} \quad (44)$$

The accuracy of the Linear Response Model can be checked at the end by a direct comparison of the model response in the center of the variation domain compared to a calculation with the parameter at their reference value.

Several responses have been selected such as total pressure (P_{tot}), mean gas temperature (T_m), condensation mass flow rate on the three condensers (Q_c), spurious condensation ($Q_{c,s}$), the difference between

	P_{tot} (bars)	T_m (^{o}C)	$Q_{c,low}$ (g/s)	$Q_{c,med}$ (g/s)	$Q_{c,up}$ (g/s)	$Q_{c,s}$ (g/s)	$\triangle T_{h/b}$ (^{o}C)	$\triangle T_{sat,h}$ (^{o}C)	$\triangle T_{sat,b}$ (^{o}C)	$u_{z,max}$ (m/s)	$u_{z,min}$ (m/s)
a_0 (1)	3.314	124.96	30.95	34.88	42.86	21.28	8.49	3.07	9.25	1.68	-0.26
a_1, M_{air}	**1.44**	0.03	-0.23	-0.63	-0.05	0.69	-4.39	6.95	-1.73	0.29	-0.57
a_2, Q_{st}	0.18	0.11	4.16	2.8	2.26	-0.89	3.42	-3.58	1.57	1.14	1.2
a_3, T_{inj}	-0.03	0.31	-0.35	0.68	-0.24	0.05	5.76	6.89	7.2	1.8	1.7
a_4, $T_{c,up}$	0.56	0.23	7.67	8.31	**-12.87**	0.87	-3.33	7.11	-0.36	-0.66	-0.76
a_5, $T_{c,m}$	0.45	0.21	9.87	**-15.78**	5.6	1.03	2.58	-4.51	0.27	-0.88	-0.76
a_6, $T_{c,l}$	0.56	0.28	**-17.75**	7.29	6.94	1.02	0.64	0.98	1.17	-0.8	0.51
a_7, l_m	-0.4	-0.5	7.72	-0.34	-4.9	-1.34	**-30.03**	21.66	-12.41	**-26.31**	**7.77**
a_8, h_{ext}	-1.07	-0.28	-10.41	-9.83	-9.41	**50.8**	2.03	4.45	2.95	0.48	0.25
a_9, h_{conv}	0.0	**-1.67**	-1.59	0.45	-0.56	1.2	-2.36	**-76.22**	**-27.05**	2.0	1.89
a_{10}, $C_{p,s}$	0.03	0.32	0.2	-0.12	0.48	0.01	3.23	8.96	5.75	-0.35	0.69
a_{11}, h_l	0.15	0.02	0.42	0.54	0.9	-3.87	-3.52	4.83	-0.77	1.35	0.82
Ref. (2)	3.303	124.07	32.66	33.69	41.99	21.65	7.57	2.64	8.2	1.49	-0.26
(1-2)/(2)	0.003	0.007	-0.052	0.035	0.021	-0.017	0.122	0.163	0.128	0.129	0.01

Table 4: Results of the sensitivity study (red bold font is ised to highlight the main contributors and Ref. corresponds to the 2D verification of the linear response model).

the temperatures at (0.95m,1.575m) and (0.95m, 7.125m) (in the system of coordinates having its origin at the floor center, OX - along a radius and OY - along the axis of symmetry), difference between T_{gas} and T_{sat} at the points (0.95m, 1.575m) and (0.95m, 7.125m) ($\triangle T_{sat,b}$ and $\triangle T_{sat,h}$,respectively) and the minimum and the maximum vertical velocity at the LDV radius at the height 4.3m. The results of the sensitivity study are reported on Table 4 The different coefficients in the main table (a_1 to $a_1 1$) are expressed in terms of % of the selected response Y_i.
Before any interpretation, it is very interesting to check the validity of the LRM by a comparison of the results of the LRM in the center of the variation domain (a_0 coefficient) and the corresponding 2D calculation. The errors for the global variables are quite satisfactory (below 5%), the maximum values are related to the condensation mass flow rates on the three condensers and these are the responses which are strongly connecteso the interactions between parametere have to be taken into account if one wants to obtain more accurate results.
The total pressure mainly depends on the initial mass of air and the accurate simulation of the heat losses. The mean gas temperature is mainly driven by the convective heat exchange along the condensers (energy transfer without mass). Then, the mixing length acting on the mixing process of the rising jet becomes important. The condensation mass flow rate is mostly controlled by the condensers temperature. Then, the impact of the spurious condensation is evident and, finally, the mixing length becomes an important parameter (decrease of the mixing length will decrease the mixing process and enhance the condensation mass flow rate along the upper condenser). The spurious condensation is mainly driven by the external heat losses. Gas temperature difference along the R2 axis is mainly dependent on the mixing hypothesis (choice of the mixing length). Degree of saturation along the R2 axis is first controlled by the convective heat transfer coefficient along the condensers (increase of the heat transfer coefficient will lead to conditions closer to the saturation state). Velocities are as expected controlled by the choice of the mixing length (the mixing is more important for the jet zone instead of the condensation zine). These results provide some explanations of the experimental and computational results and this may give some guidelines to investigater some post-tests calculations.

3.3. Selected example: TOSQAN

The TOSQAN experiment (Figure 3) is a closed cylindrical vessel (7 m^3, i.d. 1.5 m, total height of 4.8 m, condensing height of 2 m) into which steam or non-condensable gases are injected through a vertical

pipe located on the vessel axis. This vessel has thermostatically controlled walls so that steam condensation may occur on one part of the wall (the condensing wall, CW), the other part being superheated (the non condensing wall, NCW). Over 150 thermocouples are located in the vessel (in the main flow and near the walls). 54 sampling points for mass spectrometry are used for steam volume fraction measurements [1]. Optical accesses are provided by 14 overpressure resistant viewing windows permitting non-intrusive optical measurements along an enclosure diameter at 4 different levels (LDV and PIV for the gas velocities, Raman spectrometry for steam volume fractions, [13]). Measurements are mainly located at the different positions presented in Figure 3.

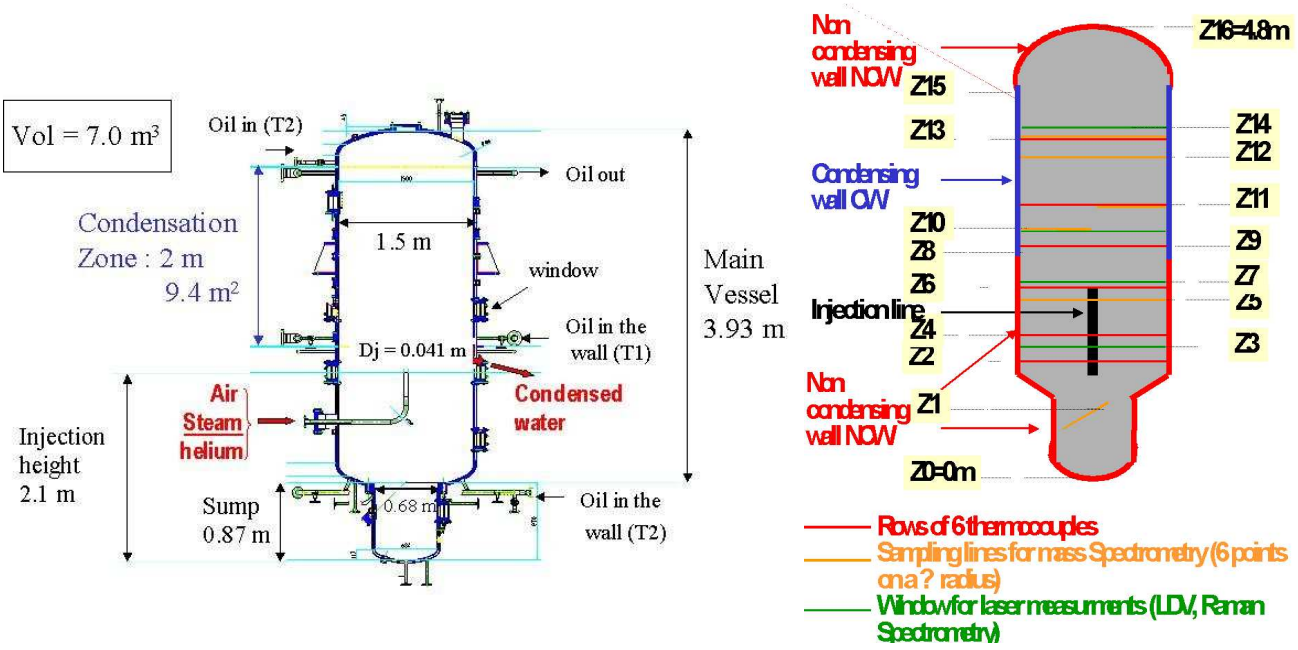

Figure 3: Schematic view of the TOSQAN facility (left) and positions of the measurements profiles available in the TOSQAN facility (right).

Condensation tests in TOSQAN consist of a water steam injection into the enclosure that is initially filled with air at atmospheric pressure, the NCW and the CW having already reached their nominal temperature. After a transient stage corresponding to enclosure pressurization, a steady-state is reached when the water steam injection and the condensation flow rates are equal. This corresponds to constant enclosure total pressure and thermal equilibrium. The TOSQAN condensation test matrix is described in [11].

A general description of the main phenomena occurring in TOSQAN during this steady-state is presented on Figure 4.

Qualification of TONUS is performed on two levels: a global level on which only the mean pressure during steady-state is evaluated, and a local level for which comparison of gas temperature, steam concentration and velocity profiles at different locations are given.

The code-experiment comparison of the total pressure is given on Figure 5. It can be seen that TONUS, for its LP as well as its CFD version, reproduces fairly well the experimental results.

Concerning local gas temperature, code-experiment comparison is given on Figure 6 and Figure 7. A vertical gas temperature obtained in a stratified TOSQAN test (test 9b) is well reproduced by TONUS-

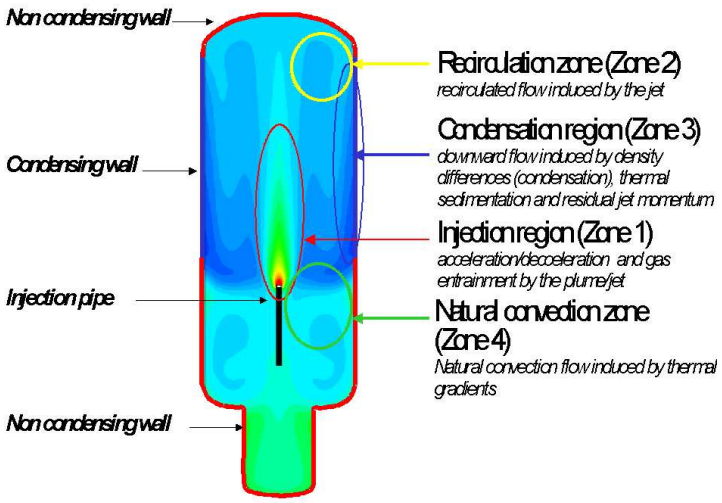

Figure 4: Schematic view of the zones corresponding to the main phenomena occurring during air-steam condensation tests (temperature field).

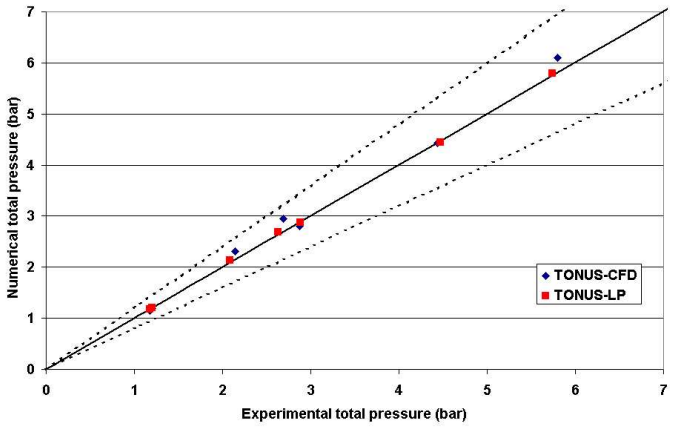

Figure 5: Mean total pressure during steady-states of all TOSQAN condensation tests.

CFD. Gas temperature horizontal profiles below the injection are also well calculated by the TONUS-CFD code. The same kind of curves can be obtained for all TOSQAN tests. The code-experiment temperature difference is generally around 1-3C.

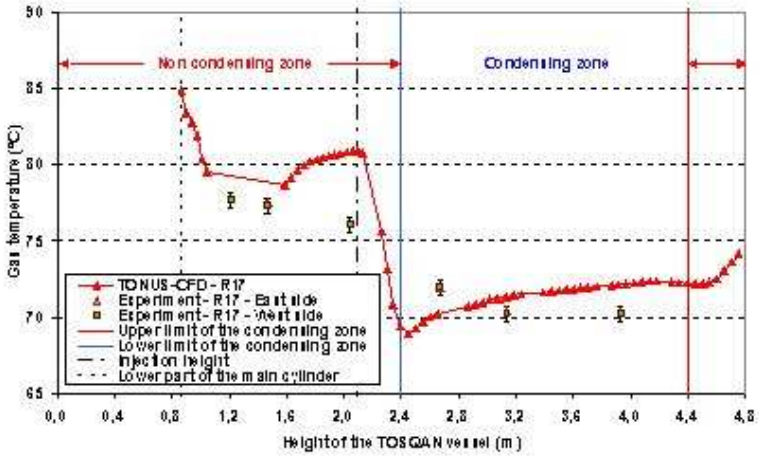

Figure 6: Vertical profile of the gas temperature at a half radius obtained during steady-state of test 9b: comparison between TONUS-CFD and TOSQAN experiments.

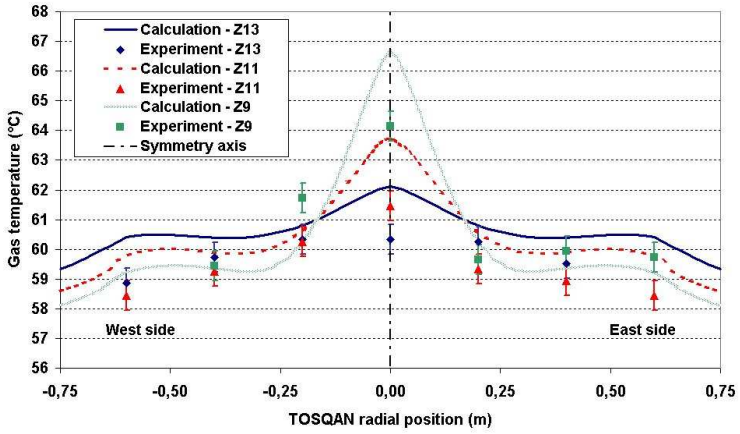

Figure 7: Horizontal profiles of the gas temperature in the jet region above the injection at heights Z9, Z11 and Z13, obtained during steady-state of test 7: comparison between TONUS-CFD and TOSQAN experiments.

An example of steam volume fractions calculated with TONUS-CFD compared to the TOSQAN experiments is given in Figure 8. The difference between code and experiment is generally below 3 % vol for the steam volume fraction. However, it should be emphasized that less experimental results are available on concentration measurements (compared to gas temperatures), so that the TONUS qualification on TOSQAN tests, specifically for gas concentrations on stratified tests, should be investigated more in depth in a near future.

Velocity measurements are also performed in TOSQAN and an example of the code-experiment comparison is given on Figure 9. There is a slight asymmetry in the experiment that explains the differences

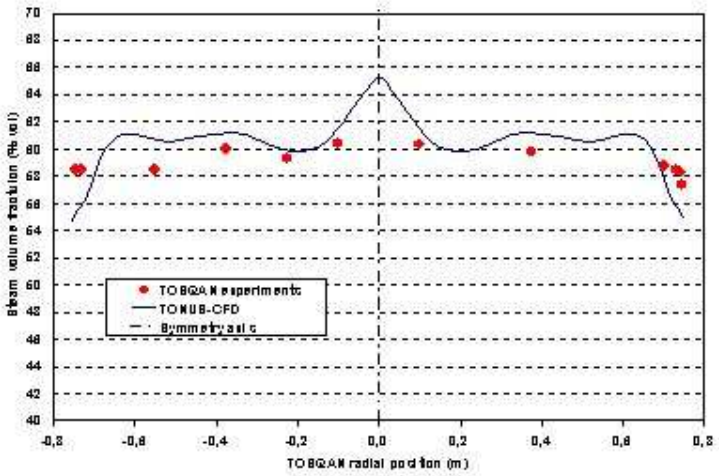

Figure 8: Horizontal profile of the steam volume fraction above the injection, obtained during steady-state of the ISP-47 (steady-state 2): comparison between TONUS-CFD and TOSQAN experiments.

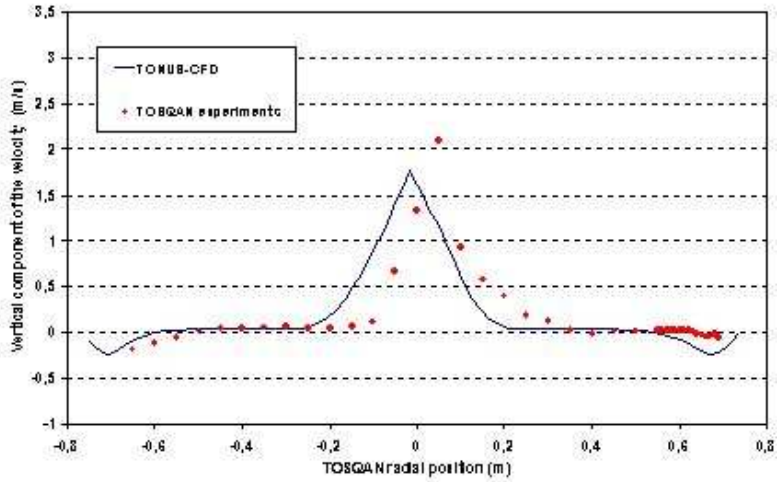

Figure 9: Horizontal profile of the vertical component of the velocity above the injection, obtained during steady-state of the ISP-47 (steady-state 2): comparison between TONUS-CFD and TOSQAN experiments.

observed on this figure. As for concentration, velocity measurements have been performed only on two tests (ISP-47 and test 1), so that the TONUS qualification on TOSQAN tests for the velocity is not so large as for gas temperatures. Code-experiment comparison on velocities under plume configuration, near the walls and under impinging jet conditions should still be performed.

3.4. Selected example: RUT STM4

The RUT facility, located in the Russian Research Center of the Kurchatov Institute, is devoted to hydrogen combustion and detonation studies. The full reinforced concrete RUT facility has three regions:

- a first channel partially obstructed by twelve obstacles of the blockage ratio (BR) 30% is 34.6 m long, 2.3 m high and 2.5 m wide. The left end of the channel is closed with 70 t steel plates.
- a second channel with a straight part and a final curved part. The total length of the channel is about 18 m - other dimensions being unchanged.
- a canyon between the first channel and the second one. The two channels open at the top of the canyon. The canyon is a rectangular room which is 10.6 m long, 6.3 m high and 2.5 m wide.

The sketch of the facility is presented on the figure 10. The geometrical positions of the pressure transducers are presented on the figure 11.

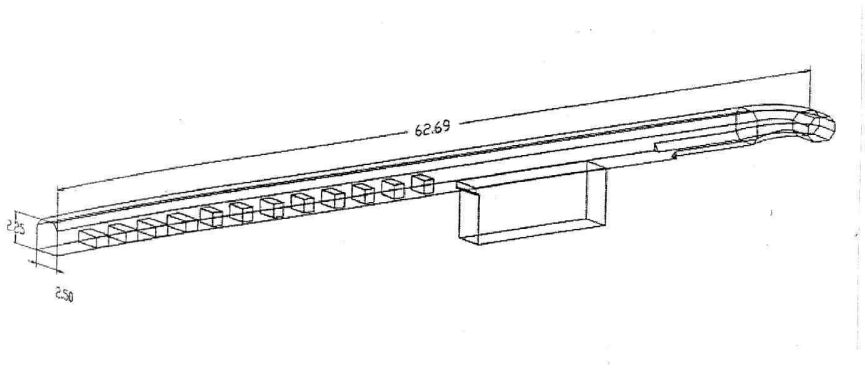

Figure 10: **The RUT geometry**.

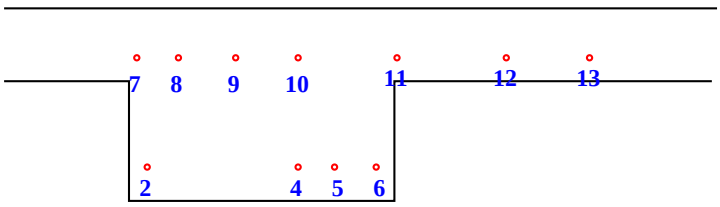

Figure 11: Transducers positions.

For the STM4 test case the initial pressure is fixed at 1 bar. The initial temperature is constant and maintained at 90^{o}C. Air (21% of oxygen and 79% of nytrogen), steam and hydrogen are initially present in the facility. The initial molar fractions are 24.8% for steam and 24.8 % for hydrogen in dry air. Experimentally the ignition takes place at the beginning of the first channel. The resulting flame front accelerates due to the presence of obstacles in the first channel. At its end the flame speed reaches the

value of 894 m/s and we observe a deflagration to detonation transition (DDT). Inside the canyon the detonation is stable and the detonation front velocity reaches a value of 1610 m/s.

Numerical studies have been performed only for the detonation phase, i.e. the flame ignition and acceleration are not considered. For the computation we only model the canyon and the second channel in two spacial dimensions. We consider three meshes: coarse mesh of 675 element, finer mesh of 14682 elements and the finest mesh of 29352 elements (see figure 12). On the figure 13 we compare the pressure

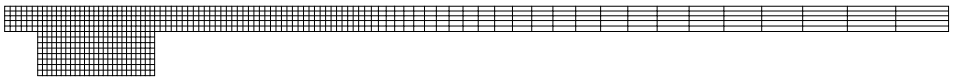

Figure 12: The coarse grid of 675 elements. (The finest grid consists of 29352 elements).

histories at the transducer 10 computed using three grids. The convergence studies show that for this test case it is sufficient to have about 15000 elements in order to capture the main features of the flow.

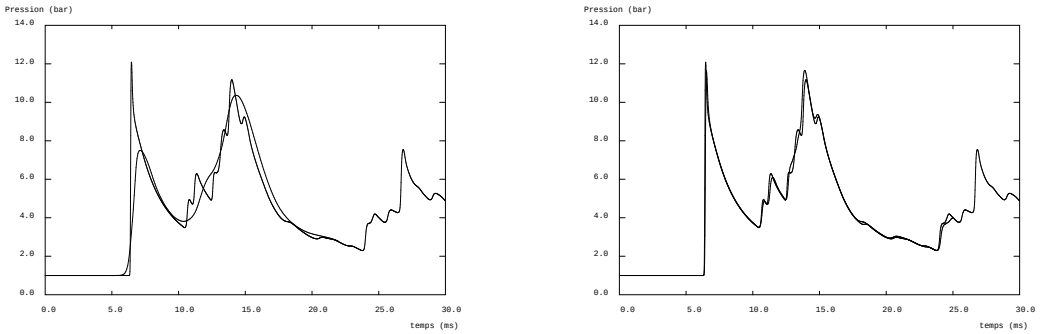

Figure 13: Comparison of the pressure histories computed on the coarse and the finest grids (left), and on the fine and the finest grids (right) (transducer 10).

This mesh would give the characteristic size of a computational cell of the order of 10 cm. Experimental studies have shown that the size of a detonation cell is of the order of 50 cm, i.e. there are at least a few computational cells per detonation cell.

The Arrhenius detonation model was chosen for the numerical experiment.

$$\dot{\omega} = A \cdot H(T - T_{th}) \cdot \rho_{H_2}^c \cdot \rho_{O_2} \cdot T^{-b} \cdot exp(-T_a/T) \tag{45}$$

where T_{th} is taken to be 600 K for this case.

Numerical validation here is based on comparisons between the computed and experimentally measured pressure histories at the pressure transducers locations. On the figure 14 we present the comparisons at the transducers 5 (left) and 8 (right); the qualitative behaviour of the curves at the other transducers is similar to those two. We can observe (see figure 14) an adequate correlation between the computed and measured pressure histories. The saw-like behaviour of the experimental curves can be explained by the three-dimensional effects (shock-lateral walls interractions).

The sensitivity on T_{th} studies have been performed for this test. Three more computations, for $T_{th} = 800$ K, $T_{th} = 1000$ K and $T_{th} = 1500$ K, have been realised. The results for $T_{th} = 800$ K are almost identical to those for $T_{th} = 600$ K. The significant differences appear for $T_{th} \geq 1000$ K. In particular, the pressure peaks are lower in comparison with the solution corresponding to $T_{th} = 600$ K. At $T_{th} = 1500$ K the

shock wave and the flame front propagate separately, i.e. shock wave does not provide high enough temperature in order to ignite the mixture. This numerical phenomenon is depicted on the figure 15: the hydrogen mass fraction isovalues for $T_{th} = 1500$ K are different from those corresponding to $T_{th} = 600$ K.

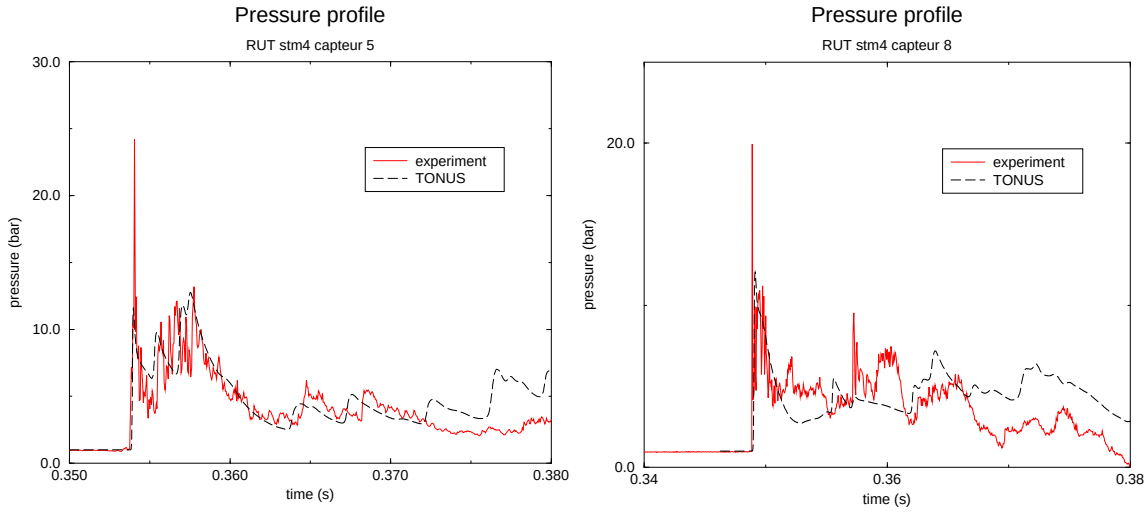

Figure 14: Pressure histories taken at the transducer 5 (left) and 8 (right).

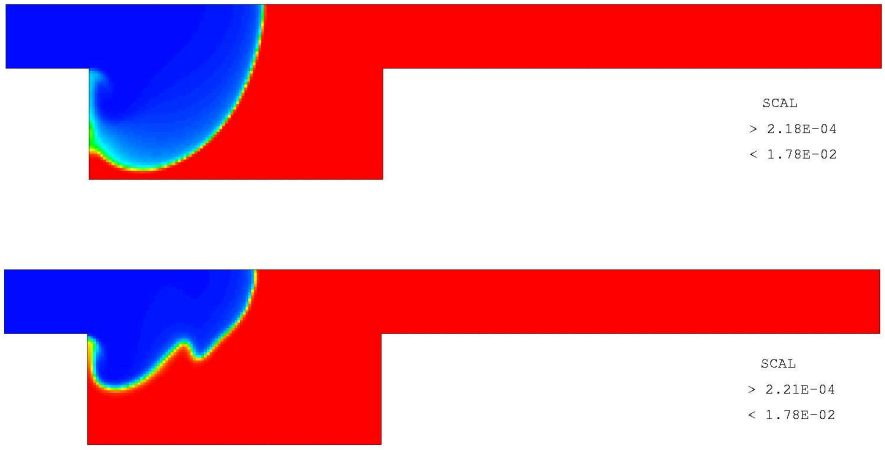

Figure 15: Hydrogen mass fraction at 5 ms for $T_{th} = 600$ K (top) and for $T_{th} = 1500$ K (bottom)

4. Analysis of the hydrogen risk in the reactor containment

French EPR design uses the so called ”two room concept”; containment is separated in two parts, a relatively small inaccessible part, hosting all the primary circuit components, and a large accessible part. The two parts are connected by rupture discs and flaps that are closed in normal operating conditions. In case of loss of coolant accident, the pressure increase in the containment causes the failure of the

rupture discs and opening of the flaps connecting the two rooms of the containment. These connections have an important safety function as they promote the establishment of large convection loops in the containment and avoid local high hydrogen concentrations. Rupture discs fail under a given pressure difference between the two rooms; flaps open passively on criteria based on the absolute pressure level in the containment. The passive flaps opening mechanism assures that the total flaps surface is always available to connect the two rooms in case of pressure increase in the containment (the flaps also open in case of loss of electric power supply).

Presently, IRSN uses the TONUS CFD code to support the hydrogen risk assessment for the EPR plants and to investigate the impact of the two room concept on hydrogen distribution in the EPR containment. Several sequences have been identified as the most threatening for the hydrogen risk in the reactor containment. It consists of sequences characterised by a large in-vessel hydrogen mass production and high hydrogen release rate. For these sequences the hydrogen behaviour in the containment is analysed. In particular, the impact of the ”two room concept” is analysed with a special attention to the uncertainties concerning the number and position of failed rupture discs. For each identified sequence the analysis is thus repeated for different assumptions concerning the open connections between the two rooms of the containment.

For the needs of the analyses, a mesh generating procedure of the containment atmosphere of EPR has been used. This procedure makes use of the user interface language of TONUS (GIBIANE) and easily allows mesh refinement in regions crucial for the considered transient. The mesh actually used for the EPR distribution computations has approximately 80 000 cells. Figure 16 shows a detail of some internal surface delimiting the containment atmosphere.

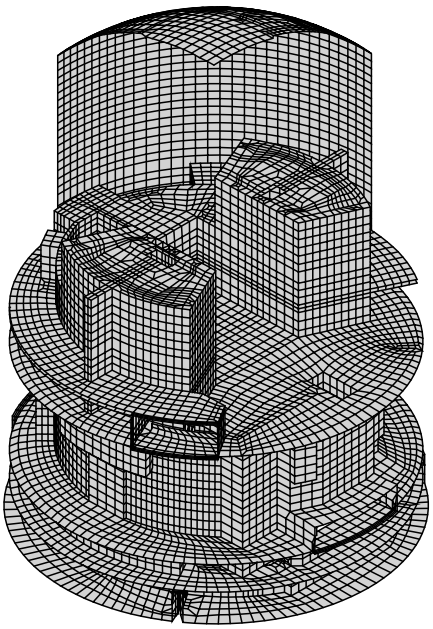

Figure 16: Details of some internal surface delimiting the gas volume

The analysis of hydrogen distribution in the reactor containment is carried out in order to determine first the extension of the flammable region during the transient (See figure 17). When flammability conditions are met in the reactor containment, the risk for internal structures or for the reactor building to be threatening by hydrogen combustion is evaluated using flame acceleration σ-criterion [6]. The region where the risk of flame acceleration exists is then identified and the evaluation of the pressure loads on the reactor building and on internal structures is obtained by performing combustion computation using

the CREBCOM model. The location and the instant of flame ignition are chosen to lead to the worst consequences for the containment.

The comparison of results obtained for the same accidental sequence with different assumptions concerning the number and position of failed discs allow determination of sensitivity of results to this aspect and to assess whether or not the retained solution met the safety requirements.

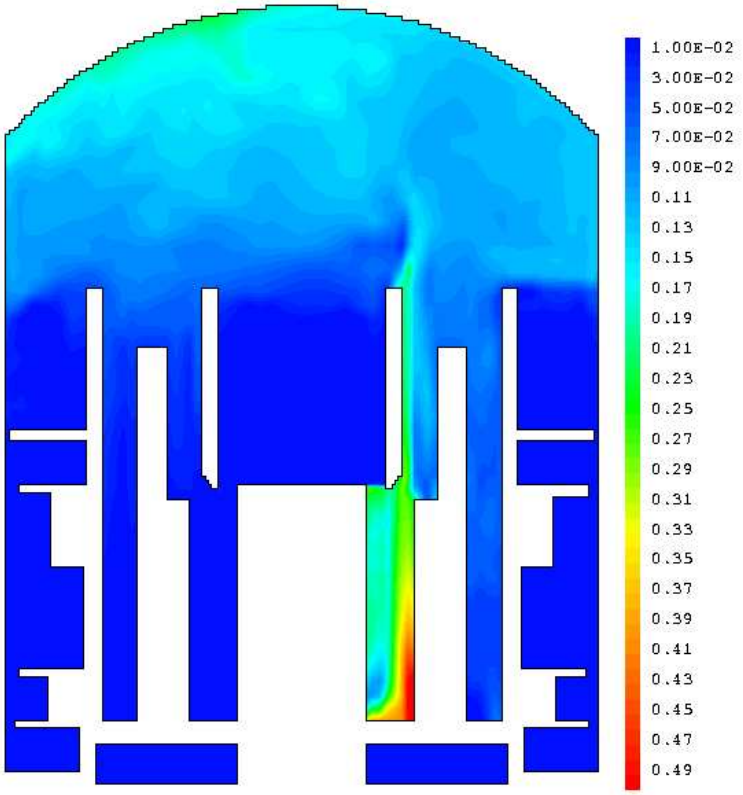

Figure 17: Example of computed hydrogen distribution in the reactor containment

5. Conclusions

In this paper, the physical models and numerical schemes implemented in the version v2006.1 of the TONUS CFD code are presented. The test cases which form the basis of the code validation are reviewed and some examples of sensitivity analyses for some of these cases are detailed, highlighting the importance of applying Best Practice Guidelines specific for Containment applications.

The on-going work related to the code development includes (a) turbulence modelling in order to have better resolution of the local fields and (b) improvements in the combustion models which will make them more predictive. Interpretations of the MISTRA (tests M5 and M6), TOSQAN (spray tests) and EPR plant applications tests are under way and the related results will be reported in the near future.

References

[1] O. Auban, J. Malet, P. Brun, J. Brinster, J.J. Quillico, E. Studer, *Implementation of gas concentration measurement systems using mass spectrometry in containment thermal-hydraulics test facilities: different approaches for calibration and measurement with steam/air/helium mixtures*, 10th International Topical Meeting on Nuclear Reactor Thermal Hydraulics (NURETH-10), Seoul, Korea, 2003.

[2] A. Beccantini et al., *Simulation of hydrogen release and combustion in large scale geometries: models and methods, Int. Conf. on SuperComputing for Nuclear Applications*, SNA-2003, Paris, 22-24 September, 2003

[3] A. Beccantini, H. Paillère, P. Morel and F. Dabbene, *Multi-dimensional simulation of hydrogen detonations*, 17th ICDERS, Heidelberg, 1999.

[4] D. Benoist, Y. Tourbier and S. Germain-Tourbier, *Plans d'Expriences: Construction et analyse*, Technique & Documentation - Lavoisier, 1994.

[5] R.B. Bird, W.E. Stewart, E.N. Lightfoot, *Transport phenomena*, Wiley, 1960.

[6] W. Breitung et al.,1999, *OECD State-of-the-Art Report on Flame Acceleration and Deflagration-to-Detonation Transition in Nuclear Safety*, NEA/CSNI/R(2000)7 (2000).

[7] T. Cron, E. Hansjosten, A. Silde, and L. Wolf, *Investigations on Hydrogen Deflagration in a Reactor Containment*, Versuche E12.1.1-E12.3.3. Technical Report No. 118-93 (November 1993). HDR-Sicherheitsprogramm. Kernforschungszentrum Karlsruhe GmbH, Germany.

[8] A.A. Efimenko and S.B. Dorofeev, 2001, *CREBCOM code system for description of gaseous combustion*, Journal of Loss Prevention in the Process Industries pp. 575-581.

[9] H. Fogt, A. Kneer and V. Seidl, *Three-Dimensional Paralle Numerical Calculation of Pressure Loads Generated by Hydrogen Deflagration in Complex Geometries*, In Proceedings of ICONE 5: 5^{th} International Conference on Nuclear Engineering, May 26-30, 1997, Nice, France

[10] J. Guermond, Mathematical Modelling and Numerical Analysis **30(5)**, 637 (1996).

[11] J. Malet, E. Porcheron, J. Vendel, *Filmwise condensation applied to containment studies: conclusions of the TOSQAN air-steam condensation tests*, the 11th International Topical Meeting on Nuclear Reactor Thermal-Hydraulics (NURETH-11), Avignon, France, October 2-6, 2005.

[12] S. Paolucci, *On the filtering of the sound waves from the Navier-Stokes equations*, Techn. Report, Sandia National Laboratories, SAND82-8257 (1982).

[13] E. Porcheron, L. Thause, J. Malet, P. Cornet, P. Brun, J. Vendel, *Simultaneous application of spontaneous Raman scattering and LDV, PIV for steam/air flow characterization*, 10th International symposium on flow visualization, Kyoto, Japan, 2002.

[14] D.B. Spalding, 1971, *Mixing and Chemical Reaction in Steady Confined Turbulent Flames*, In *13th Symp. (Int.) on Combust.*, The Combustion Institute, Pittsburgh, pp. 649-657.

[15] E. Studer, F. Dabbene, J.P. Magnaud, L. Blumenfeld, J.J. Quillico and H. Paillère, *On the use of the MISTRA Coupled Effect Test Facility for the Validation of Containment Thermal-Hydraulics Codes*, NURETH-10, Seoul, Korea, Oct. 2003.

[16] E. Studer et al., *International Standard Problem on Containment Thermal-hydraulics ISP47 - Step 1. Synthesis of MISTRA exercise*, submitted Nucl. Eng. Design, 2006

[17] J.R. Travis, 1987, *A Heat, Mass and Momentum Transport Model for Hydrogen Flames in Nuclear Reactor Containments*, Nuclear Engineering and Design, **101**, pp. 149-166.